environmental microbiology

Environmental Microbiology (2017) **19**(3), 1041–1053 doi:10.1111/1462-2920.13605

Integrated proteomics and metabolomics suggests symbiotic metabolism and multimodal regulation in a fungal-endobacterial system

Zhou Li,[1,6] Qiuming Yao,[1] Stephen P. Dearth,[2] Matthew R. Entler,[3,4] Hector F. Castro Gonzalez,[2] Jessie K. Uehling,[5] Rytas J. Vilgalys,[5] Gregory B. Hurst,[6] Shawn R. Campagna,[2] Jessy L. Labbé[4] and Chongle Pan[1,3,4]*

[1]*Computer Science and Mathematics Division, Oak Ridge National Laboratory, Oak Ridge, TN, USA.*

[2]*Department of Chemistry, University of Tennessee, Knoxville, TN, USA.*

[3]*Graduate School of Genome Science and Technology, University of Tennessee-Oak Ridge National Laboratory, Knoxville, TN, USA.*

[4]*Biosciences Division, Oak Ridge National Laboratory, Oak Ridge, USA.*

[5]*Department of Biology, Duke University, Durham, NC, USA.*

[6]*Chemical Sciences Division, Oak Ridge National Laboratory, Oak Ridge, TN, USA.*

Summary

Many plant-associated fungi host endosymbiotic endobacteria with reduced genomes. While endobacteria play important roles in these tri-partite plant–fungal–endobacterial systems, the active physiology of fungal endobacteria has not been characterized extensively by systems biology approaches. Here, we use integrated proteomics and metabolomics to characterize the relationship between the endobacterium *Mycoavidus* sp. and the root-associated fungus *Mortierella elongata*. In nitrogen-poor media, *M. elongata* had decreased growth but hosted a large and growing endobacterial population. The active endobacterium likely extracted malate from the fungal host as the primary carbon substrate for energy production and biosynthesis of phospho-sugars, nucleobases, peptidoglycan and some amino acids. The endobacterium obtained nitrogen by importing a variety of nitrogen-containing compounds. Further, nitrogen limitation significantly perturbed the carbon and nitrogen flows in the fungal metabolic network. *M. elongata* regulated many pathways by concordant changes on enzyme abundances, post-translational modifications, reactant concentrations and allosteric effectors. Such multimodal regulations may be a general mechanism for metabolic modulation.

Received 1 September, 2016; revised 8 November, 2016; accepted 16 November, 2016. *For correspondence. E-mail panc@ornl.gov; Tel. (+865) 574 1281.

Introduction

A major component of plant microbiomes include fungi, whose activities have significant impact on the productivity and health of their plant hosts (Bonfante and Anca, 2009). Many plant-associated fungi in turn host symbiotic bacteria within their cells. Endobacteria have been found in root endophytic fungi (Sharma *et al.*, 2008), ectomycorrhizal fungi (Bertaux *et al.*, 2005) and arbuscular mycorrhizal fungi (Ghignone *et al.*, 2012; Naito *et al.*, 2015; Torres-Cortes *et al.*, 2015). Previous studies have shown that endobacteria can boost fungal energy production (Salvioli *et al.*, 2016), increase fungal sporulation success (Salvioli *et al.*, 2016), promote plant growth (Sharma *et al.*, 2008) and enhance plant resistance to pathogenic fungi (Sharma *et al.*, 2008). The tri-partite interactions in these plant–fungal–endobacterial systems constitute critical symbiotic links in terrestrial ecosystems (Bonfante and Anca, 2009).

However, little is known about these endobacteria beyond their reduced genomes (Lackner *et al.*, 2011; Ghignone *et al.*, 2012; McCutcheon and Moran, 2012; Fujimura *et al.*, 2014; Naito *et al.*, 2015; Torres-Cortes *et al.*, 2015) (Uehling *et al.*, Under Review of Environmental Microbiology). Due to the low endobacterial biomass relative to the fungal biomass in their co-cultures, active metabolic processes of growing endobacteria have not been systematically characterized. Open questions include how endobacteria obtain carbon and nitrogen from their fungal hosts and how the imported nutrients are metabolized to produce energy and build endobacterial biomass. In this study, we observed that nitrogen limitation significantly increased the population of the endobacterium *Mycoavidus* sp. in the root-associated fungus *Mortierella*

elongata strain AG-77 (Gottel *et al*., 2011; Shakya *et al*., 2013; Ohshima *et al*., 2016) (Uehling *et al*., Under Review of *Environmental Microbiology*). This allowed for a comprehensive proteomics study of an active endobacterium within a fungal host. The results uncovered the key carbon and nitrogen compounds imported from the fungal host and the metabolic pathways used by the endobacterium for energy production and biosynthesis.

We then combined proteomics (Wu and MacCoss, 2002; Aebersold and Mann, 2003; Li *et al*., 2012) and metabolomics (Dettmer *et al*., 2007; Bowen and Northen, 2010; Steffen *et al*., 2014; Wang *et al*., 2014) to characterize the metabolic responses of the fungal host to nitrogen limitation, and to antibiotic treatment to suppress the endobacterium (Uehling *et al*., Under Review of *Environmental Microbiology*). For major pathways in the fungal host, we quantified the constituent intermediates, the interconversion enzymes, the phosphorylation and acetylation of these enzymes and the allosteric effectors of these enzymes. The holistic measurements of these pathways uncovered many examples of multimodal regulation achieved by concordant actions on multiple regulatory switches of linked pathways. We found nitrogen limitation dramatically altered the nitrogen and carbon flows in the fungal metabolic network.

Results

Proteomic and metabolomic measurements of a M. elongata*/*Mycoavidus *sp. symbiotic system*

In this study, *M. elongata* was grown with a normal endobacterial population (B+) or a suppressed endobacterial population (B−) in a nitrogen-rich medium (N+) or a nitrogen-poor medium (N−) for a total of four conditions designated as N+B+, N−B+, N+B− and N−B+. The growth curves of the cultures in the four conditions were measured for a period of 96 h (Supporting Information Fig. 1). The biomass production was highest in the N+B− condition, followed by N+B+, then N−B− and finally N−B−. The culture growth in all four conditions transitioned from the exponential phase to the stationary phase after approximately 72 h (Supporting Information Fig. 1). Separate sets of cultures were grown for 72 h in the four conditions in biological triplicates and harvested for proteomics and metabolomics measurements.

The proteomics results are shown in Table 1 and Supporting Information Data 1. The numbers of peptide-spectrum matches (PSMs), peptide identifications, protein identifications, phosphorylation events and acetylation events are tabulated by fungal proteins and endobacterial proteins in the four conditions in Table 1. In total, proteomics identified 34% of proteins encoded in the fungal genome and 32% of proteins encoded in the endobacterial genome. Phosphorylation events were found on 4%–7%, and acetylation events on 10%–13%, of the identified proteins (Supporting Information Data 2). Fungal proteins accounted for 93.5%–99.9% of the total number of PSMs in the four conditions (Table 1), which likely reflected the dominance of fungal biomass over endobacterial biomass in these cultures. Because of this, metabolomics measurements were considered to reflect fungal metabolomes. A total of 92 metabolites were identified and quantified in the four growth conditions (Supporting Information Fig. 2 and Supporting Information Data 3). The Pearson correlations between biological replicates were 0.94 ± 0.03 for protein abundances and 0.96 ± 0.05 for metabolite abundances. Nitrogen limitation and endobacterium suppression significantly changed the abundances of many proteins and metabolites and the fractional occupancies of post-translational modification (PTM) events (Supporting Information Table 1 and Supporting Information Data 4–6). All fold changes referred to in the Results section below had significant p values < 0.05 and q values < 0.05.

The relative abundance of the endobacterium in the symbiotic system was estimated using unique PSMs from endobacterial proteins (Table 1). The antibiotics treatment effectively suppressed the relative abundance of the endobacterium to 0.04% in both growth media. Without the antibiotics treatment, nitrogen limitation significantly increased the relative abundance of the endobacterium by 17 fold (from 0.38% in N+B+ to 6.5% in N−B+). The 64 endobacterial proteins identified in the N+B+ condition were common high-abundance proteins, such as ribosomal proteins, elongation factor, RNA polymerase, GroEL and

Table 1. Summary statistics of proteomics results in the four growth conditions.

Conditions	N+B+		N+B−		N−B+		N−B−	
Proteomics identifications	Fungus	Endo-bacterium	Fungus	Endo-bacterium	Fungus	Endo-bacterium	Fungus	Endo-bacterium
PSM	246,907	929	239,962	108	299,575	21,025	317,046	111
Peptide	54,559	428	55,441	90	60,033	6,163	51,395	91
Protein	4,264	64	4,297	4	4,557	683	4,014	6
Phosphorylation	374	1	325	4	284	25	261	0
Acetylation	733	12	882	2	761	46	800	4

PSM: peptide-spectrum match.

DnaK. The 683 endobacterial proteins identified in the N−B+ condition covered many processes of endobacterial metabolism. Identification of endobacterial proteins involved in DNA replication (e.g. DNA polymerase, helicase and gyrase) and cell division (e.g. ftsZ) indicated the active multiplication of the endobacterium in the N−B+ condition. Proteomics identified all endobacterial enzymes in the TCA cycle except for the indistinguishable

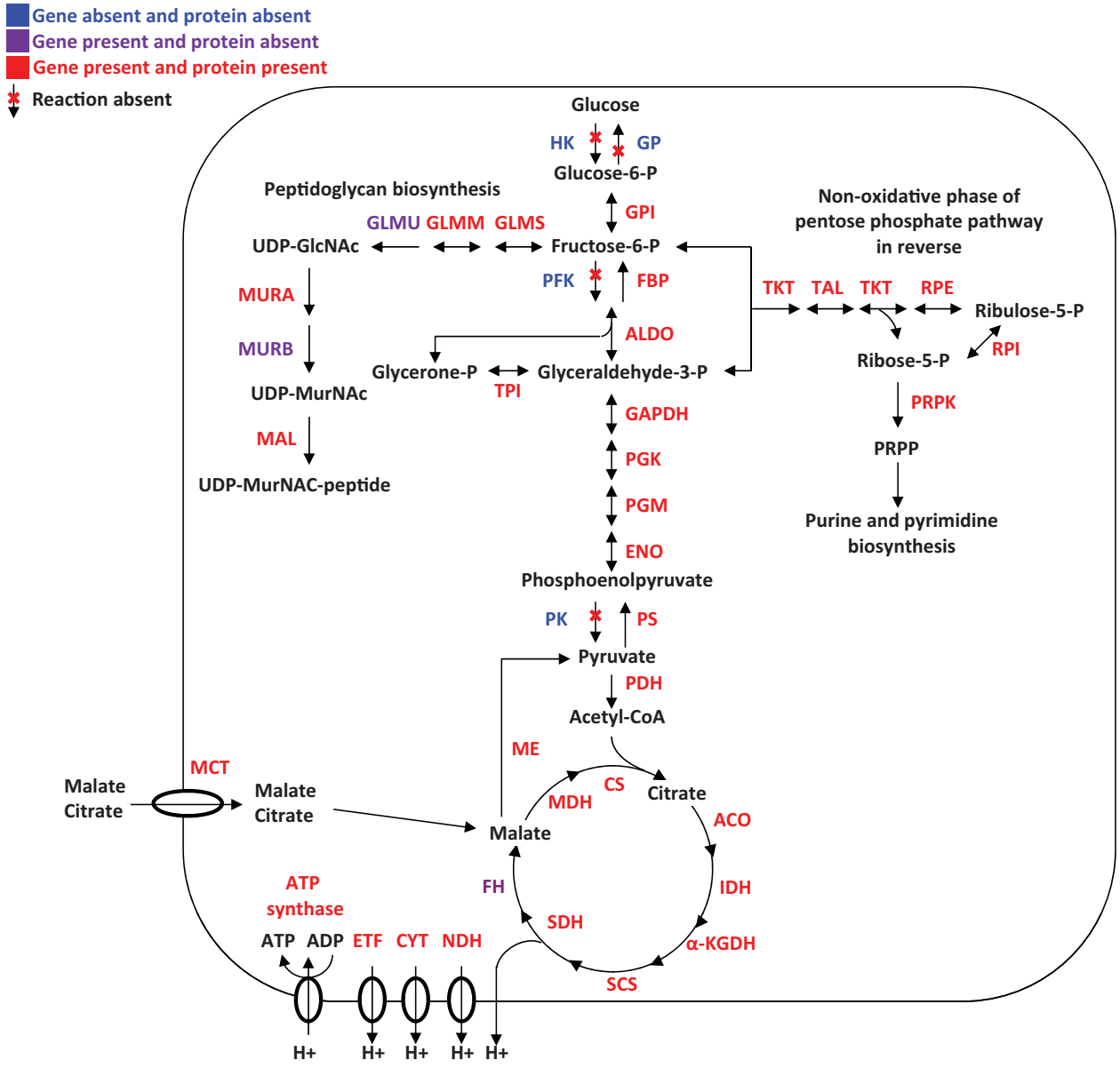

Fig. 1. Reconstructed core metabolic network of the active endobacterium. Malate was imported from the fungal host to drive the TCA cycle and supply the gluconeogenesis pathway. The TCA cycle produced NADH for the electron transport chain. The gluconeogenesis pathway provided carbon substrate for other biosynthesis pathways. HK: hexokinase; GP: glucose-6-phosphatase; GPI: glucose-6-phosphate isomerase; PFK: phosphofructokinase; FBP: fructose-1,6-bisphosphatase; ALDO: fructose-bisphosphate aldolase; TPI: triose-phosphate isomerase; GAPDH: glyceraldehyde-3-phosphate dehydrogenase; PGK: phosphoglycerate kinase; PGM: phosphoglycerate mutase ENO: enolase; PK: pyruvate kinase; PS: phosphoenolpyruvate synthase; PDH: pyruvate dehydrogenase; CS: citrate synthase; ACO: aconitate hydratase; IDH: isocitrate dehydrogenase; α-KGDH: α-ketoglutarate dehydrogenase; SCS: succinyl-CoA ligase; SDH: succinate dehydrogenase; FH: fumarate hydratase; MDH: Malate dehydrogenase; ME: malic enzyme; MCT: malate/citrate transporter; NDH: NADH dehydrogenase; CYT: cytochromes; ETF: electron transfer flavoprotein-ubiquinone oxidoreductase; GLMS: glutamine-fructose-6-phosphate aminotransferase; GLMM: phosphoglucosamine mutase; GLMU: UDP-N-acetylglucosamine pyrophosphorylase/glucosamine-1-phosphate N-acetyltransferase; MURA: UDP-N-acetylglucosamine 1-carboxyvinyltransferase; MURB: UDP-N-acetylenolpyruvoylglucosamine reductase; MAL: UDP-N-acetylmuramate amino acid ligases; TKT: transketolase; TAL: transaldolase; RPE: ribulose-5-phosphate-3-epimerase; RPI: ribose-5-phosphate isomerase; and PRPK: ribose-phosphate diphosphokinase.

fumarate hydratase (FH) (endobacterial FH and fungal FH have an identical protein sequence) and a complete suite of enzymes for electron transport chain (Fig. 1). Enzymes for biosynthesis of ubiquinone were also identified by proteomics in the endobacterium. This suggested that the endobacterium maintained independent ATP production through an active TCA cycle and electron transport chain. Thus, the proteomics results of the N−B+ condition illustrated the metabolism of an actively multiplying endobacterial population within a nitrogen-constrained fungal host.

Core carbon metabolism of the active endobacterium

The endobacterium requires a supply of a carbon substrate from its fungal host to sustain its TCA cycle and electron transport chain in the N−B+ condition. Glucose was the primary carbon source in the growth medium (dextrose-yeast broth). As hypothesized in previous studies (Zientz *et al*., 2004; Ghignone *et al*., 2012), the endobacterium may use imported glucose through the glycolysis pathway to drive its TCA cycle. As illustrated in Fig. 1, the glycolysis pathway shares seven enzymes for the reversible reactions with the gluconeogenesis pathway; however, key glycolysis enzymes required to carry out the three irreversible, rate-limiting steps in glycolysis are missing from the endobacterial genome (Uehling *et al*., Under Review of *Environmental Microbiology*), including hexose kinase (HK), phosphofructokinase (PFK) and pyruvate kinase (PK). Because the endobacterial genome is a closed genome, the absence of these genes cannot be explained by incomplete genome reconstruction. Therefore, glucose cannot serve as the primary carbon substrate for endobacterial energy production.

The endobacterial genome contains 12 distinct malate/citrate transporter genes (MCT) (Uehling *et al*., Under Review of *Environmental Microbiology*). Encoding these many genes for malate/citrate transportation in such a reduced genome suggests a high evolutionary pressure for the endobacterium to maintain its ability to extract malate or citrate from the fungal host. While shotgun proteomics has technical bias against membrane proteins, one of these transporters was identified by proteomics. Although malate and citrate are intermediates in the TCA cycle, they cannot directly enter the TCA cycle as intermediates, because that would result in an unsustainable open TCA cycle with the accumulation of other intermediates. We did not find a pathway for citrate to enter the TCA cycle via acetyl-CoA. However, proteomics identified a malic enzyme (ME) that can convert malate to pyruvate and all subunits of the pyruvate dehydrogenase (PDH) complex that can convert pyruvate to acetyl-CoA (Fig. 1). These two enzymes would allow malate to enter the TCA cycle through acetyl-CoA. Thus, we hypothesize that the endobacterium may import malate to supply acetyl-CoA for the TCA cycle and other biosynthesis pathways.

To produce malate for the endobacterium, the fungal host was found to encode two malate synthases (MS) in the genome, separate from fumarase that converts fumarate to malate in the fungal TCA cycle. In the N−B+ condition relative to the N−B− condition, proteomics measured a 14-fold increase for one of the malate synthases (q value = 0.048), while metabolomics found no significant change in the concentration of malate. Thus, relative to the N−B− condition, the large endobacterial population in the N−B+ condition likely increased the demand for malate, which in turn stimulated the production of malate by the fungal host through the malate synthase. The proportionally increased supply and consumption of malate balanced at the same level of malate between the two conditions.

Biosynthesis of key carbon compounds in the active endobacterium

Biosynthesis or import of an array of carbon compounds was needed to support the active multiplication of the endobacterium in the N−B+ condition. Intermediates in the glycolysis and gluconeogenesis pathways are important precursors for many biosynthesis pathways. The endobacterium was not able to use glycolysis to produce those intermediates from glucose (Fig. 1). Instead, proteomics identified all enzymes in the gluconeogenesis pathway from pyruvate to glucose-6-phosphate, including phosphoenolpyruvate synthase (PS) and fructose-1,6-bisphosphatase (FBP) for the two key irreversible reactions of gluconeogenesis. The endobacterial genome encodes all 24 enzymes for purine and pyrimidine biosynthesis (Supporting Information Fig. 3). All these enzymes except PurN and PyrE were identified by proteomics.

Ribose-5-phosphate needed for Phosphoribosyl pyrophosphate (PRPP) biosynthesis is generally produced from glucose-6-phosphate via the pentose phosphate pathway. The pentose phosphate pathway typically consists of an oxidative phase and a subsequent non-oxidative phase (Supporting Information Fig. 4). Interestingly, the three enzymes in the oxidative phase are not encoded in the endobacterial genome, while all four enzymes in the non-oxidative phase are encoded in the genome and identified by proteomics (Fig. 1). Thus, the normal substrate of the non-oxidative phase, ribulose-5-phosphate, cannot be generated by the oxidative phase. However, the normal products of the non-oxidative phase, glyceraldehyde-3-phosphate and fructose-6-phosphate, were being produced by the active gluconeogenesis pathway as described above. Because the four enzymes in the non-oxidative phase catalyze reversible reactions, we believe the endobacterium produced ribose-5-phosphate from glyceraldehyde-3-phosphate and fructose-6-phosphate by operating the non-oxidative phase of pentose phosphate pathway in reverse (Fig. 1).

Biosynthesis and import of key nitrogen compounds in the active endobacterium

The growing endobacterium is able to carry out active protein synthesis from amino acids. Proteomics identified all aminoacyl-tRNA synthetases encoded in the endobacterial genome, with the exception of asparaginyl-tRNA synthetase. Supporting Information Table 2 summarizes the genomic presence and the proteomic identification of the enzymes required for amino acid synthesis. Proteomics identified the full suite of enzymes required for the synthesis of glycine, alanine, leucine, isoleucine, valine, glutamate and aspartate. A number of amino acid transporters are encoded in the endobacterial genome and identified by proteomics (Supporting Information Table 2). Additionally, proteomics also identified di-peptide transporter and peptidase for digesting fungal peptides into amino acids.

Spermidine/putrescine and 4-aminobutyrate (GABA) are important nitrogen-containing compounds. The endobacterial genome also encodes 13 spermidine/putrescine transporting genes and a GABA permease gene. Out of these, proteomics identified eight spermidine/putrescine transporting proteins and the GABA permease.

Peptidoglycan for cell wall construction was synthesized from amino sugars (i.e. *N*-acetyl-D-glucosamine and *N*-acetyl-muramic acid) and amino acids. All five enzymes for the biosynthesis of these two amino sugars from fructose-6-phosphate are encoded in the endobacterial genome. Three of these enzymes were identified by proteomics. Furthermore, a set of ligases that sequentially add amino acids to *N*-acetyl-muramic acid were also identified by proteomics. These results suggested that the endobacterium might be able to actively build its cell wall through independent biosynthesis of its constituent amino sugars from fructose-6-phosphate (Fig. 1).

Glutathione is consumed by glutathione S-transferase (GST) for detoxification and is produced by gamma-glutamylcysteine synthetase (GCS) and glutathione synthetase (GSS) (Anderson, 1998). The endobacterium expressed GST in its proteome, but lacked the GCS and GSS genes in its genome for glutathione synthesis. Fungal GCS and GSS were identified by proteomics and glutathione was detected by metabolomics. Thus, the endobacterial GST probably utilizes glutathione imported from the fungal host.

Impact of the multiplying endobacterium on the fungal host

The proteome and metabolome of the fungal host were compared between the N−B+ condition and the N−B− condition. Because these two conditions used the same growth medium, the physiological changes of the fungal host can be attributed to the effects of an abundant multiplying endobacterial population in the N−B+ condition versus a suppressed endobacterial population in the N−B− condition.

Chitin is a structural component of the fungal cell wall. The abundance of several intermediates in the chitin biosynthesis pathway, including *N*-acetyl-glucosamine-1-phosphate/*N*-acetyl-glucosamine-6-phosphate and UDP-*N*-acetyl-glucosamine, decreased by 1.4-fold (q value = 0.032) and 2.0-fold (q value = 0.043) respectively in N−B+ relative to N−B−. Chitin can be deacetylated to chitosan by chitin deacetylase (Zhao *et al.*, 2010). The abundance of chitin deacetylase increased by 4.7-fold (q value = 0.049) in N−B+ versus N−B−. These results suggested that the endobacterial presence may affect the synthesis and structure of fungal cell wall.

Effects of nitrogen limitation on the key nitrogen metabolism of M. elongata

The N+B+ condition and the N−B+ condition were compared to uncover the effects of nitrogen limitation on the fungal host with an endobacterial population. Glutamate is one of the central nitrogen donors for intracellular nitrogen metabolism (Miflin and Habash, 2002). Figure 2 shows the nitrogen transfers between glutamate and the other key compounds involved in nitrogen metabolism. Nitrogen limitation significantly changed the abundances of many of these compounds and their interconversion enzymes (Fig. 2), which indicated a major perturbation of the nitrogen flows in *M. elongata* by nitrogen limitation.

Glutamate was converted to glutamine at a higher rate in N−B+ relative to N+B+. Three copies of glutamine synthetase (GS) catalyzing an irreversible reaction from glutamate to glutamine were 3.4-, 2.4- and 1.6-fold more abundant (q value = 0.008, 0.026 and 0.019 respectively). Glutamate was 2.9-fold (q value = 0.00007) more abundant, providing more substrate for GS. Correspondingly, ferredoxin-dependent glutamate synthase (FDGS) was 4.1-fold (q value = 0.01) less abundant, preventing a reversible reaction between glutamine and glutamate. But the concentration of glutamine was 2.6-fold (q value = 0.0024) lower. If the concentrations of glutamine in both conditions were at a steady state (i.e. the same number of glutamine was produced and consumed, holding its concentration constant), the consumption rate of glutamine probably increased despite a lower availability of glutamine in N−B+ relative to N+B+.

Alanine aminotransferase (ALT) catalyzes a reversible conversion between alanine and glutamate. Proteomics showed an up-regulation of two copies of ALT by 6.0- and 2.1-fold (q value = 0.023 and 0.021 respectively) in N−B+ relative to N+B+, but provided no information on whether the substantially larger conversion was from alanine to glutamate or in the opposite direction. Since metabolomics

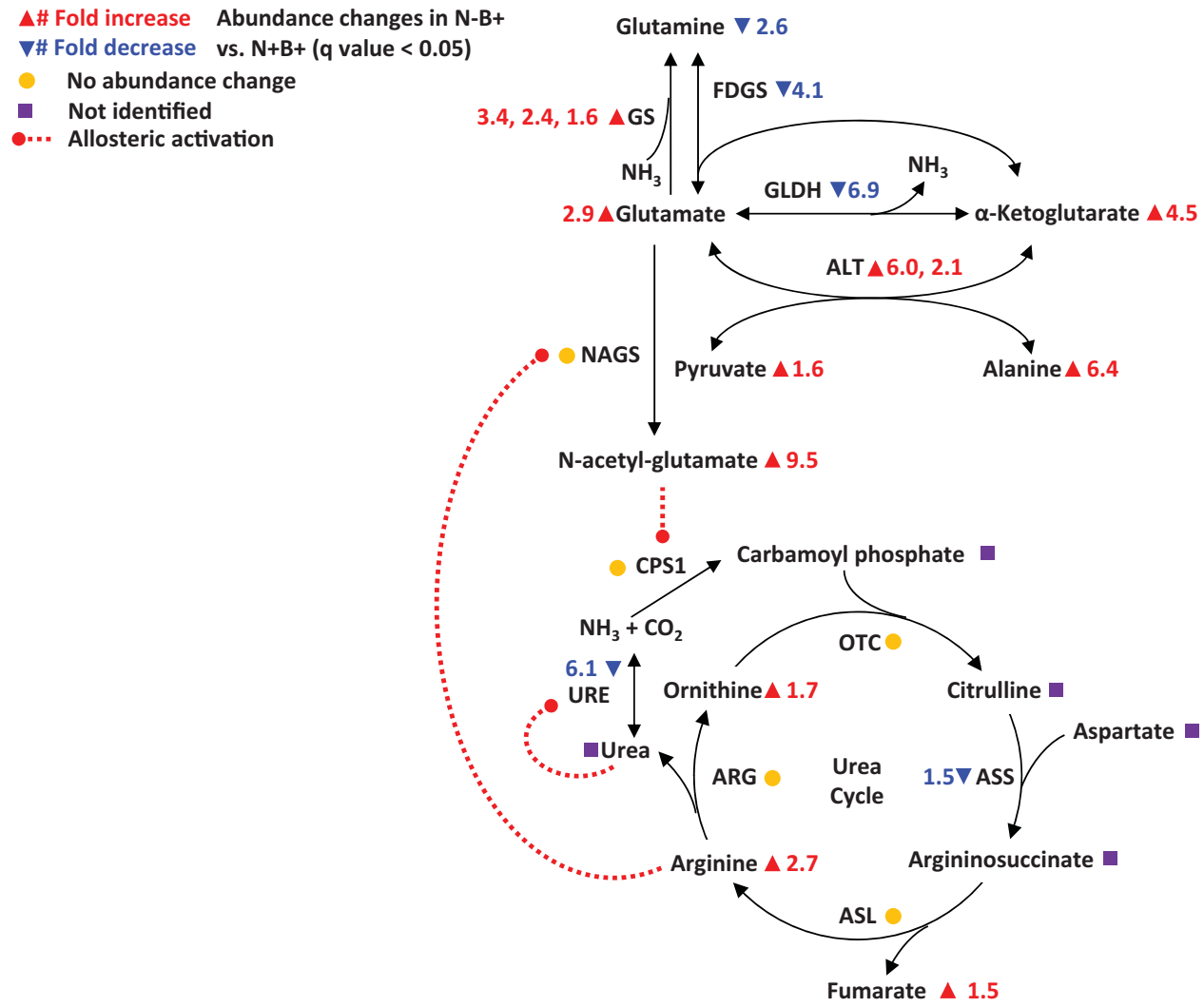

Fig. 2. Multimodal regulation of the nitrogen-metabolism pathways in the fungal host in response to nitrogen limitation. *M. elongata* increased the nitrogen flow from alanine to glutamate and from glutamate to glutamine and *N*-acetyl-glutamate through enzyme abundance changes and reactant concentration changes. NH_3 was converted to urea at higher rate by allosteric activation of the urea cycle and lower expression of the urease. GS: glutamine synthetase; FDGS: ferredoxin-dependent glutamate synthase; GLDH: glutamate dehydrogenase; ALT: alanine aminotransferase; NAGS: N-acetylglutamate synthase; CPS1: carbamoyl phosphate synthetase I; OTC: ornithine transcarbamylase; ASS: argininosuccinate synthase; ASL: argininosuccinate lyase; ARG: arginase; and URE: urease.

measured all reactants of ALT, we calculated the fold change of the reaction quotients of ALT in the two conditions by:

$$\frac{Q_{N-B+}}{Q_{N+B+}} = \frac{F_{Alanine} \times F_{\alpha-Ketoglutarate}}{F_{Pyruvate} \times F_{Glutamate}} = 6.2$$

where $F_{Alanine}$, $F_{\alpha\text{-Ketoglutarate}}$, $F_{Pyruvate}$ and $F_{Glutamate}$ are the fold changes of these reactants from N−B+ to N+B+ and Q_{N-B+} and Q_{N+B+} are the reaction quotients of ATL in N−B+ and N+B+ respectively. The 6.2-fold increase of the reaction quotient in N−B+ relative to N+B+ suggests that ALT probably converted alanine to glutamate in N−B+ and the reaction rate was much higher with higher level of enzymes and substrates.

The urea cycle is a central conduit in the nitrogen metabolism and it is also coupled with the metabolism of glutamate. *N*-Acetylglutamate synthase (NAGS) had no significant abundance change, but could be activated by a 2.7 fold (q value = 0.0021) higher concentration of arginine (Caldovic *et al.*, 2006), an intermediate in the urea cycle. Since the activation of NAGS resulted in 9.5 fold (q value = 0.0036) more abundant *N*-acetylglutamate in N−B+, which is an allosteric activation of the first enzyme of the urea cycle (Morris, 2002), we

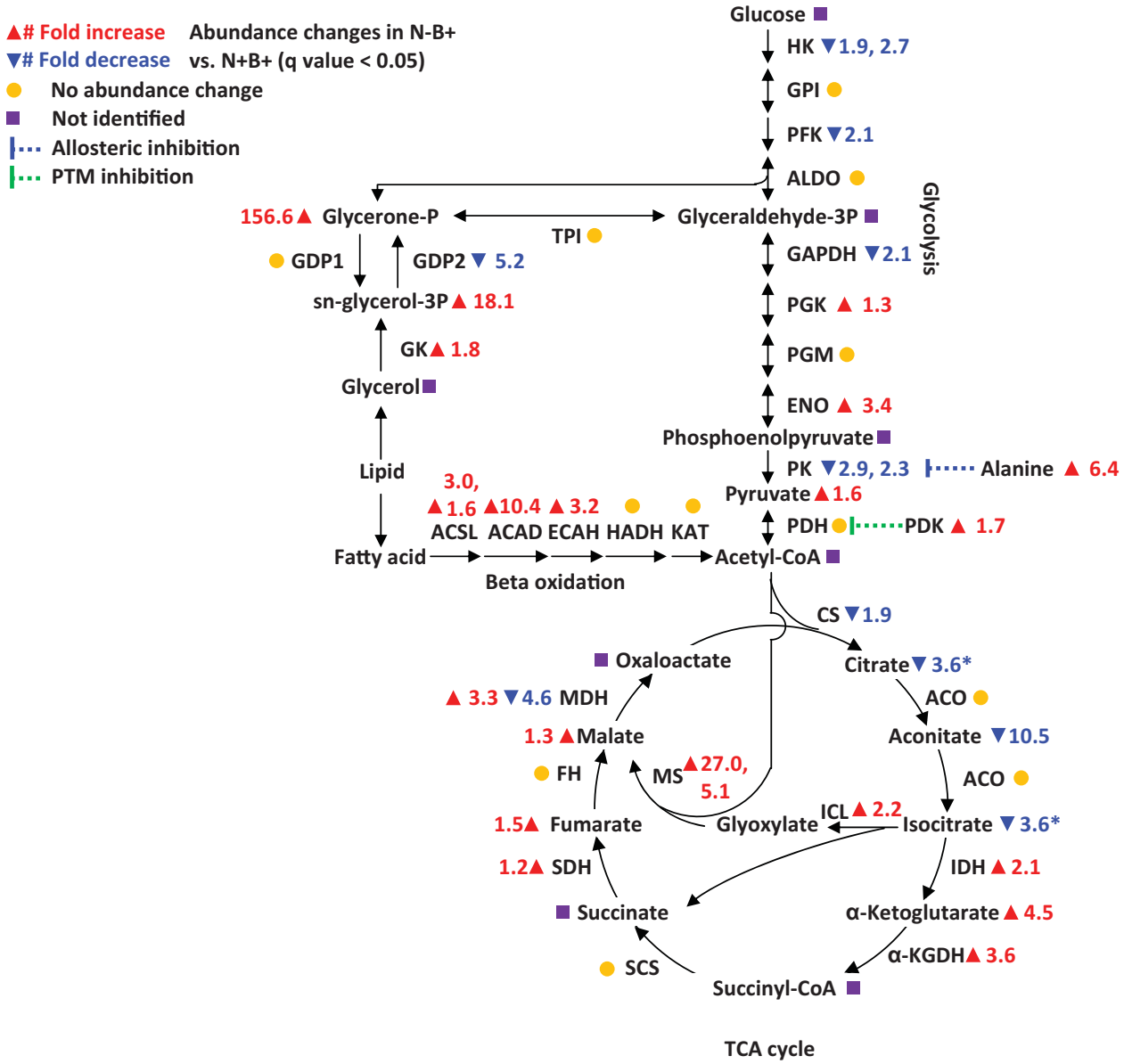

Fig. 3. Multimodal regulation of the carbon-metabolism pathways of the fungal host in response to nitrogen limitation. *M. elongata* increased beta-oxidation of fatty acids by higher enzyme expression and suppressed glycolysis by decreasing abundances of HK, PFK and PK, allosteric inhibition of PK and phosphorylation of PDH. *M. elongata* also enhanced the malate production through higher abundances of malate synthases to support a larger endobacterial population. The asterisk indicates citrate and isocitrate were indistinguishable by metabolomics. HK: hexokinase; GPI: glucose-6-phosphate isomerase; PFK: phosphofructokinase; ALDO: fructose-bisphosphate aldolase; TPI: triose-phosphate isomerase; GAPDH: glyceraldehyde-3-phosphate dehydrogenase; PGK: phosphoglycerate kinase; PGM: phosphoglycerate mutase; ENO: enolase; PK: pyruvate kinase; PDH: pyruvate dehydrogenase; PDK: pyruvate dehydrogenase kinase; GDP: glycerol-3-phosphate dehydrogenase; GK: glycerol kinase; ACSL: long-chain-fatty-acid-CoA ligase; ACAD: acyl-CoA dehydrogenase; ECAH: enoyl-CoA hydratase; HADH: 3-hydroxyacyl-CoA dehydrogenase; KAT: β-ketothiolase; CS: citrate synthase; ACO: aconitate hydratase; IDH: isocitrate dehydrogenase; α-KGDH: α-ketoglutarate dehydrogenase; SCS: succinyl-CoA ligase; SDH: succinate dehydrogenase; FH: fumarate hydratase; MDH: malate dehydrogenase; ICL: isocitrate lyase; and MS: malate synthase.

hypothesize the urea cycle might be allosterically activated to convert NH_3 to urea. In line with the higher synthesis rate of urea from NH_3, the hydrolysis of urea back to NH_3 might be turned down with a 6.1 fold (q value = 0.001) abundance decrease of urease (URE) in N−B+ relative to N+B+.

Effects of nitrogen limitation on the carbon metabolism of M. elongata

The carbon metabolism of *M. elongata* was also perturbed by nitrogen limitation in the N−B+ condition compared to the N+B+ condition (Fig. 3). We quantified all enzymes in

the fungal TCA cycle by proteomics and 6 out of 9 intermediates by metabolomics. These enzymes and intermediates had divergent abundance changes in N−B+ relative to N+B+, reflecting the alterations of carbon flows between the TCA cycle and other pathways by nitrogen limitation.

The three key regulatory enzymes in the fungal glycolysis pathway (i.e. HK, PFK and PK, Fig. 3) were quantified to have reduced abundance in N−B+ relative to N+B+. In addition, the nitrogen limitation increased the abundance of alanine by 6.4 fold (q value = 0.0012). Alanine is an allosteric inhibitor of PK (Alontaga and Fenton, 2011), suggesting that the irreversible conversion of phosphoenolpyruvate to pyruvate might be suppressed by decreased abundance and allosteric deactivation of PK. Furthermore, the immediate next step from pyruvate to acetyl-CoA might also be suppressed by the phosphorylation of pyruvate dehydrogenase (PDH) without significant abundance change (Korotchkina and Patel, 1995). This evolutionarily conserved phosphorylation event can inhibit the activity of PDH in many different organisms (Yao *et al.*, 2012; 2014) (Supporting Information Fig. 5). Proteomics revealed that the fractional occupancy of this phosphorylation event (i.e. the percentage of phosphorylated copies out of all copies of PDH) increased from 7% in N+B+ to 38% in N−B+ (q value = 0.029). Consistent with the increased fractional occupancy, pyruvate dehydrogenase kinase that phosphorylated PDH was found to have 1.7 fold (q value = 0.036) higher abundance in N−B+ relative to N+B+. Because of the suppression of the three irreversible steps of glycolysis and the deactivation of pyruvate dehydrogenase, nitrogen limitation probably down-regulated the carbon flow from glucose to the TCA cycle.

Nitrogen limitation significantly up-regulated the abundances of the first three enzymes in the beta-oxidation pathway (Fig. 3). This suggests that beta-oxidation of fatty acids was probably activated to compensate for the diminished supply of acetyl-CoA from glycolysis pathway. The fatty acids were probably generated from lipid degradation with a co-production of glycerol. Substantial accumulation of glycerol degradation products, sn-glycerol-3-phosphate and glycerone-phosphate, were found in N−B+ relative to N+B+. While there were no lipids or fatty acids provided in the growth media, lipid staining showed substantial amounts of lipids in the fungal cells from all four growth conditions (Supporting Information Fig. 6). Thus, nitrogen limitation probably activated the degradation of the lipid reserve in this growth stage, despite abundant glucose remaining in the growth media.

Discussion

Fungal–bacterial endosymbiosis is an important ecological phenomenon that occurs across many types of plant-associated fungi (Bonfante and Anca, 2009). However, functional characterization of endobacteria living with fungal hosts has been a challenge, because they often have very low relative biomass abundance in co-cultures. In two previous pioneering studies, 6 proteins (Salvioli *et al.*, 2010) and 24 proteins (Vannini *et al.*, 2016) were identified from the endobacterium of an arbuscular mycorrhizal fungus, *Gigaspora margarita*. By exposing the *M. elongata*/*Mycoavidus* sp. symbiotic system to nitrogen limitation, we increased the relative abundance of endobacterial biomass in the co-cultures and identified 683 endobacterial proteins out of a total of 2181 predicted proteins by proteomics. This proteome was biologically relevant, since nitrogen limitation is probably the normal condition for the fungal host living in a natural environment (LeBauer and Treseder, 2008) and the endobacterium was actively multiplying in the N−B+ co-culture.

We addressed the open question regarding the key carbon and energy substrates for the endobacterium in *M. elongata*/*Mycoavidus* sp. endosymbiosis. Such a substrate must have a fungal production mechanism, an active transportation system into the endobacterium and an endobacterial consumption mechanism. In the nitrogen-limiting growth condition studied here, proteomics and metabolomics provided strong support for malate as the key carbon substrate for *Mycoavidus* sp. The fungal host increased malate production by a malate synthase in the glyoxylate pathway to support an increased endobacterial population in N−B+. The endobacterium was equipped with 12 MCTs to extract malate from the fungal host. The high frequency of such transporter genes in a reduced endobacterial genome may indicate its evolutionary competition with the fungal host for the pool of malate in the fungal cells. Finally, proteomics identified a full set of enzymes that channeled an influx of malate into the TCA cycle, gluconeogenesis, the pentose phosphate pathway's non-oxidative phase in reverse and other biosynthesis pathways. These proteomics and metabolomics results generated many hypotheses for specific metabolic interactions in this biological system, which can be tested in future molecular biology experiments.

In the nitrogen-poor condition, the endobacterium obtained nitrogen from the fungal host by importing amino acids, di-peptides, spermidine/putrescine and GABA. From these nitrogen-containing compounds and carbon metabolism intermediates, the endobacterium was able to synthesize nucleic acids, peptidoglycan and amino acids. Proteomics provides evidence that the endobacterium used these building blocks to replicate DNA, synthesize proteins and construct cell wall to support its multiplication, while the fungal host had constrained growth from the nitrogen limitation. Additionally, suppression of the endobacterium by antibiotics increased the biomass productivity of *M. elongata* in both growth media

(Supporting Information Fig. 1). Thus, the endobacterium constituted significant demand, and probably autonomous competition, for scarce nutrients within *M. elongata* in the laboratory co-cultures, which is also supported by the findings by Uehling *et al.*, Under Review of *Environmental Microbiology*.

By examining the metabolic responses of *M. elongata* to nitrogen limitation, we found multiple modes for metabolic regulation, including enzyme abundance changes, protein PTMs, reactant abundance changes and small-molecule allosteric regulation. This study demonstrated how multimodal regulations on linked pathways formulated coordinated responses to a perturbation. For example, we found *M. elongata* shifted its carbon source for the TCA cycle from glucose to fatty acids in response to nitrogen limitation. This shift was accomplished by the phosphorylation deactivation of PDH, allosteric inhibition of PK and decreased abundances of three key enzymes in the glycolysis pathway, and the protein abundance increases for multiple enzymes in the beta-oxidation pathway. In the nitrogen metabolism, *M. elongata* increased the nitrogen flows from alanine to glutamate and then to glutamine in response to nitrogen limitation. The increased fluxes were achieved by simultaneously increasing the protein abundances of ALT and GS and the substrate abundances of these two enzymes. *M. elongata* also stimulated the urea cycle from NH_3 to urea using two coupled allosteric activators and simultaneously suppressed the conversion of urea back to NH_3 by decreasing the abundance of urease.

In total, we found *M. elongata* responded to nitrogen limitation by re-wiring its carbon and nitrogen flows. More interestingly, all of these responses were implemented through multimodal regulations that integrated multiple concordant regulatory actions on enzyme abundances, reactant concentrations, protein PTMs and allosteric effectors. Each of these regulatory modes has advantages and disadvantages. Regulation by enzyme abundance provides direct control on a specific reaction, but incurs energy cost and time lag in production and degradation of enzymes. Regulation by reactant concentrations can change the direction of reversible reactions and substrate availability, but affects other reactions that share their reactants. Regulation by protein PTMs and allosteric effectors are efficient and fast, but may be feasible only for enzymes that have evolved to have such flexibility to switch on and off their activities by PTMs or small-molecule binding. Because an organism may choose different optimum regulatory modes for different reactions across linked pathways, we hypothesize that multimodal regulation may be the norm for metabolic regulation in systems biology. While this may not be apparent in previous studies using a single omics analysis, our study found multiple examples by integrating proteomics and metabolomics.

Experimental procedures

Growth of M. elongata *cultures in four conditions*

Stock cultures of *M. elongata* strain AG-77 with a normal population of the endobacterium *Mycoavidus* sp. (B+) were maintained in potato-dextrose agar (PDA) (Sigma Aldrich, St. Louis, MO). Stock cultures with a suppressed endobacterial population (B−), obtained from the Vilgalys lab, were created as described previously(Uehling *et al.*, Under Review of *Environmental Microbiology*) and were maintained in PDA with 60 $\mu g\ ml^{-1}$ Kanamycin, Streptomycin and Chloramphenicol. The stock cultures were propagated every 10 days to fresh PDA plates.

For this study, the N+B+ cultures were grown from the natural stock cultures (B+) in potato-dextrose broth (PDB) that contained abundant nitrogen (N+). The N+B− cultures were grown from the cleared stock cultures (B−) in PDB (N+) with 60 $\mu g\ ml^{-1}$ Kanamycin, Streptomycin and Chloramphenicol. The N−B+ cultures were grown from the natural stock cultures (B+) in dextrose-yeast broth (DYB) with only 1% yeast extract (N−) (Sigma Aldrich, St. Louis, MO). The N−B− cultures were grown from the cleared stock cultures (B−) in dextrose-yeast broth (DYB) with only 1% yeast extract (N−) and 60 $\mu g\ ml^{-1}$ Kanamycin, Streptomycin and Chloramphenicol.

Triplicate cultures were grown for each condition in 250 ml Erlenmeyer flasks containing 50 ml of sterile growth medium for 72 h at 25°C with shaking at 120 rpm. Cell cultures in flasks were harvested on 40 um nylon basket strainers and then flash-frozen using liquid nitrogen. Frozen cell pellets were ground into power for extraction of proteins and metabolites.

To measure the growth curves of *M. elongata* in the four conditions, twelve replicate cultures were grown as described above for each condition. Every 24 h, three replicate cultures from each condition were removed from the incubator and filtered at ambient pressure through strainers. Cultures were rinsed with 5 ml deionized water and placed in a forced air incubator at 55°C until weight measurements were stable (~12 h). Culture masses were measured on a calibrated Mettler Toledo analytical balance (±0.0015 g) (Mettler Toledo, Columbus, OH).

Fluorescent imaging

For each condition, live cell imaging was performed using a Zeiss 710 laser scanning confocal microscope (Carl Zeiss, Oberkochen, Germany). Staining solution was prepared in individual microcentrifuge tubes by diluting 10 µl of 50 mg l^{-1} Nile Red/methanol in 250 ml Tris-acetate-EDTA (TAE) buffer (40 mM Tris, 20 mM acetic acid, 1mM EDTA). Approximately 2 mm^3 of mycelium was torn from the fungal pellet using tweezers and placed in the prepared staining solution. Samples were gently agitated at room temperature for 30 min. Biomass was removed from the staining solution using tweezers, rinsed in fresh TAE for 10 min by gentle agitation and placed on a glass slide. Samples were covered with a glass coverslip, tamped with tweezers to ensure uniform mycelial thickness and the coverslip was then mounted and sealed using a mixture of valap(Waterman-Storer 2001) (1:1:1[w/w/w] vasoline, parafilm, lanolin). Images were collected using a 488 nm laser

excitation wavelength, 539–753 nm detection wavelengths and a 63× oil immersion objective lens.

Proteomics measurements

The 12 proteome samples from triplicate cultures of the four conditions were prepared in parallel, as described previously (Li *et al.*, 2014). Briefly, for each culture, 150 mg of ground biomass were boiled and sonicated in 1 ml of 4% SDS (weight) dissolved in Tris buffer (100 mM, pH 8.0) (Sigma Aldrich, St. Louis, MO). Extracted proteins were precipitated in 20% (volume) trichloroacetic acid (Sigma Aldrich, St. Louis, MO), washed with ice-cold acetone (Sigma Aldrich, St. Louis, MO) three times and then re-solubilized in guanidine (6 M) (Sigma Aldrich, St. Louis, MO) and dithiothreitol (10 mM) (Sigma Aldrich, St. Louis, MO). Bicinchoninic acid assays were used to measure protein concentration prior to adding dithiothreitol. About 50 μg proteins from each culture were further cleaned up and digested by trypsin on 30 kDa molecular-weight-cutoff filters (Wiśniewski *et al.*, 2009; Li *et al.*, 2014) (Sartorius, Göttingen, Germany).

Liquid chromatography-tandem mass spectrometry (LC-MS/MS) measurements were performed, as described previously (Li *et al.*, 2014). Briefly, 25 μg of peptides from each culture were loaded offline into a two-dimensional (reverse phase and strong cation exchange) back column, washed offline and then connected to a reverse phase front column. A 11-step online multidimensional protein identification technology (MudPIT) (Washburn *et al.*, 2001) coupled with high-resolution tandem mass spectrometry was used for proteome measurements on an LTQ Orbitrap Elite mass spectrometer (Thermo Scientific, San Jose, CA). Both MS spectra and higher-energy collisional dissociation (HCD) MS/MS spectra were measured in Orbitrap. The mass spectrometry proteomics data have been deposited to the ProteomeXchange Consortium via the PRIDE partner repository with the dataset identifier PXD003240.

Proteomics data analysis

A protein sequence database was constructed from all predicted proteins in the *M. elongata* genome (BioProject Accession: PRJNA196039, and ID: 196039) and the endobactrium genome (BioProject Accession: PRJNA187127, and ID: 187127). The molecular functions of the predicted proteins in *M. elongata* and the endobacterium were predicted using the UniFam eukaryotic and prokaryotic databases respectively, as described previously (Chai *et al.*, 2014), and then used to reconstruct their metabolic networks with MetaCyc (Caspi *et al.*, 2014). Reverse sequences of all predicted proteins were added to the protein sequence database as decoys for estimation of false discovery rates (FDR) of peptide and protein identification (Elias and Gygi, 2007).

Database searching was performed with Sipros (Pan *et al.*, 2011; Hyatt and Pan, 2012; Wang *et al.*, 2013) on the Titan supercomputer at Oak Ridge Leadership Computing Facility as described previously (Li *et al.*, 2014). Briefly, parameters included parent mass offsets of −1, 0, +1, +2, +3 Da; 0.03 Da and 0.01 Da mass tolerances for parent ions and fragment ions respectively; up to three missed cleavages; a maximum of two PTMs per peptides and full enzyme specificity required. The following PTMs were dynamically searched: oxidation of methionine; phosphorylation of serine, threonine and tyrosine; and acetylation of lysine. Alkylation of cysteine by iodoacetamide was statically searched. The search result of each run was filtered to achieve 1% FDR on the peptide level. Proteins were inferred from the identified peptides using parsimony rules (Nesvizhskii and Aebersold, 2005). Indistinguishable proteins were combined into protein groups. A minimum of two peptides, at least one of which must be unique, were required for each inferred protein or protein group. PTMs were localized using the score difference (DeltaP) between the top-rank modified peptide and its next lower-ranked PTM isoform, as described previously (Li *et al.*, 2014). The FDR controlled at 1% on the peptide level were estimated to be 0.5% on the PSM level, 0.5% on the protein/protein group level and 0.7% on the PTM level.

Intensity-based label-free quantitation for protein and PTM fractional occupancy were performed with ProRata (Pan *et al.*, 2006) using peak heights from re-constructed ion chromatogram of identified peptides, as described previously (Li *et al.*, 2014). The total peak height of all quantified unique peptides from a protein was used to represent protein abundance. Student's *t* test was used to calculate *p* values for protein abundance changes, which were adjusted to *q* values for multiple comparison correction using the QVALUE package in R. A protein with both *p* value and *q* value less than 0.05 was considered significantly changed. The fractional occupancy of a PTM event on a specific residue of a protein was calculated as the ratio between the total peak height of all unique peptides carrying this PTM event and the total peak height of both modified and unmodified unique peptides covering this residue. Rank product test (Breitling *et al.*, 2004) and the QVALUE package were used to calculate the *p* values and *q* values respectively, for the changes of PTM fractional occupancies. A PTM with both *p* value and *q* value less than 0.05 was considered significantly changed.

Metabolomics

All 12 samples were prepared in parallel at 4°C unless otherwise stated. For each sample, 30 mg of ground biomass were weighed into 1.5 ml centrifuge tubes. Samples were suspended in 1.3 ml of extraction solvent (2:2:1 HPLC grade methanol, acetonitrile and water with 0.1 M formic acid) (Rabinowitz and Kimball, 2007). Extraction proceeded for 20 min at −20°C. At this point, samples were centrifuged for 5 min at 16.1 rcf. The supernatant of each sample was transferred to new vials and the biomass pellets were resuspended in 200 μl of extraction solvent. Again, the extraction proceeded for 20 min at −20°C and samples were centrifuged for 5 min at 16.1 rcf before the supernatants were transferred to their respective vials. The vials containing the 1.5 ml of combined supernatants were evaporated to dryness under a stream of N_2 gas at ambient temperature. The solid residue was then resuspended in 300 μl of sterile water and transferred to autosampler vials.

Samples were immediately moved to an Ultimate 3000 (Dionex, Sunnyvale, CA) autosampler trays maintained at 4°C. The ultra-performance liquid chromatography-mass

spectrometry (UPLC-MS) method was based off a previously described protocol from Lu and colleagues (Lu *et al*., 2008; 2010). An aliquot of 10 μl was injected into a Synergi 2.5 μm Hydro-RP 100 Å, 100 × 2.00 mm LC column (Phenomenex, Torrance, CA). The column compartment was kept at 25°C for the duration of the separation. Samples were introduced to an Exactive Plus Orbitrap (Thermo Scientific, San Jose, CA) mass spectrometer run in full-scan negative ionization mode via an electrospray ionization (ESI) source with a 0.1 mm internal diameter fused silica capillary tube. The spray voltage was set at 3 kV and the nitrogen sheath gas was set to a flow rate of 10 units with a capillary temperature of 320°C. The instrument was run with a resolution of 140,000 and an AGC target of 3e6. The scan window from 0 to 9 min was set from 85 to 800 *m*/*z* and from 9 to 25 min was set from 110 to 1000 *m*/*z*. Solvents A and B consisted of 97:3 HPLC grade water:-methanol, 10 mM tributylamine, with 15 mM acetic acid and 100% HPLC grade methanol respectively. The gradient was 0% B from 0 to 5 min, 20% B from 5 to 13 min, 55% B from 13 to 15.5 min, 95% B from 15.5 to 19 min and re-equilibrated to 0% B from 19 to 25 min. The flow rate was 200 μl min^{-1} for the entirety of the run.

Metabolomics data analysis

Spectral files generated by Orbitrap software Xcalibur (Thermo Fisher Scientific) were converted to mzML (Martens *et al*., 2011) using the ProteoWizard software package (Chambers *et al*., 2012) for data processing. MAVEN software (Clasquin *et al*., 2002; Melamud *et al*., 2010) was used to perform nonlinear retention time corrections for chromatographic data of each sample. Metabolites were manually selected on the basis of experimentally determined retention times, exact mass (± 5 ppm) and chromatographic properties (S/N ≥ 3, scans ≥ 5, Gaussian-like shape). Retention times were acquired from a previous method using identical chromatography (Lu *et al*., 2010; Luo *et al*., 2007) in addition to a customized list of standards (available upon request). Peak area counts for each of the identified metabolites were integrated for each sample for use in quantification (Supporting Information Data 3). Student's *t* test was used to estimate *p* values for metabolite abundance changes. *q* Values were calculated using the QVALUE package in R. A metabolite with both *p* value and *q* value less than 0.05 was considered significantly changed.

Acknowledgements

This work is supported by the U. S. Department of Energy (DOE), Office of Science, Office of Biological and Environmental Research, the ORNL Plant-Microbe Interfaces Scientific Focus Area project and the DOE Grant DOE-SC10010566. This research used resources of the Oak Ridge Leadership Computing Facility. Further support for S.P.D., H.F.C.G., and S.R.C. was provided through NSF award OCE-1233964. ORNL is managed by UT-Battelle, LLC, under contract DE-AC05-00OR22725 for the United States Department of Energy.

Conflict of interest

The authors declare no conflict of interest.

References

Aebersold, R., and Mann, M. (2003) Mass spectrometry-based proteomics. *Nature* **422:** 198–207.

Alontaga, A.Y., and Fenton, A.W. (2011) Effector analogues detect varied allosteric roles for conserved protein-effector interactions in pyruvate kinase isozymes. *Biochemistry* **50:** 1934–1939.

Anderson, M.E. (1998) Glutathione: an overview of biosynthesis and modulation. *Chem Biol Interact* **111:** 1–14.

Bertaux, J., Schmid, M., Hutzler, P., Hartmann, A., Garbaye, J., and Frey-Klett, P. (2005) Occurrence and distribution of endobacteria in the plant-associated mycelium of the ectomycorrhizal fungus *Laccaria bicolor* S238N. *Environ Microbiol* **7:** 1786–1795.

Bonfante, P., and Anca, I.A. (2009) Plants, mycorrhizal fungi, and bacteria: a network of interactions. *Annu Rev Microbiol* **63:** 363–383.

Bowen, B.P., and Northen, T.R. (2010) Dealing with the unknown: metabolomics and metabolite atlases. *J Am Soc Mass Spectrom* **21:** 1471–1476.

Breitling, R., Armengaud, P., Amtmann, A., and Herzyk, P. (2004) Rank products: a simple, yet powerful, new method to detect differentially regulated genes in replicated microarray experiments. *FEBS Lett* **573:** 83–92.

Caldovic, L., Lopez, G.Y., Haskins, N., Panglao, M., Shi, D., Morizono, H., and Tuchman, M. (2006) Biochemical properties of recombinant human and mouse *N*-acetylglutamate synthase. *Mol Genet Metab* **87:** 226–232.

Caspi, R., Altman, T., Billington, R., Dreher, K., Foerster, H., Fulcher, C.A., *et al*. (2014) The MetaCyc database of metabolic pathways and enzymes and the BioCyc collection of Pathway/Genome Databases. *Nucleic Acids Res* **42 (D1):** D459–D471.

Chai, J., Kora, G., Ahn, T.H., Hyatt, D., and Pan, C. (2014) Functional phylogenomics analysis of bacteria and archaea using consistent genome annotation with UniFam. *BMC Evol Biol* **14:** 207.

Chambers, M.C., Maclean, B., Burke, R., Amodei, D., Ruderman, D.L., Neumann, S., *et al*. (2012) A cross-platform toolkit for mass spectrometry and proteomics. *Nat Biotechnol* **30:** 918–920.

Clasquin, M.F., Melamud, E., and Rabinowitz, J.D. (2002). LC-MS data processing with MAVEN: a metabolomic analysis and visualization engine. *Curr Protoc Bioinformatics* (Wiley). 37:14.11:14.11.1–14.11.23.

Dettmer, K., Aronov, P.A., and Hammock, B.D. (2007) Mass spectrometry-based metabolomics. *Mass Spectrom Rev* **26:** 51–78.

Elias, J.E., and Gygi, S.P. (2007) Target-decoy search strategy for increased confidence in large-scale protein identifications by mass spectrometry. *Nat Methods* **4:** 207–214.

Fujimura, R., Nishimura, A., Ohshima, S., Sato, Y., Nishizawa, T., Oshima, K., *et al*. (2014) Draft genome sequence of the betaproteobacterial endosymbiont associated with the fungus *Mortierella elongata* FMR23-6. *Genome Announc* **2:** 01214–e01272.

Ghignone, S., Salvioli, A., Anca, I., Lumini, E., Ortu, G., Petiti, L., *et al*. (2012) The genome of the obligate endobacterium of an AM fungus reveals an interphylum network of nutritional interactions. *ISME J* **6:** 136–145.

Gottel, N.R., Castro, H.F., Kerley, M., Yang, Z., Pelletier, D.A., Podar, M., *et al*. (2011) Distinct microbial communities within the endosphere and rhizosphere of *Populus deltoides* roots across contrasting soil types. *Appl Environ Microbiol* **77:** 5934–5944.

Hyatt, D., and Pan, C. (2012) Exhaustive database searching for amino acid mutations in proteomes. *Bioinformatics* **28:** 1895–1901.

Korotchkina, L.G., and Patel, M.S. (1995) Mutagenesis studies of the phosphorylation sites of recombinant human pyruvate dehydrogenase. Site-specific regulation. *J Biol Chem* **270:** 14297–14304.

Lackner, G., Moebius, N., Partida-Martinez, L., and Hertweck, C. (2011) Complete genome sequence of *Burkholderia rhizoxinica*, an Endosymbiont of Rhizopus microsporus. *J Bacteriol* **193:** 783–784.

LeBauer, D.S., and Treseder, K.K. (2008) Nitrogen limitation of net primary productivity in terrestrial ecosystems is globally distributed. *Ecology* **89:** 371–379.

Li, Z., Adams, R.M., Chourey, K., Hurst, G.B., Hettich, R.L., and Pan, C. (2012) Systematic comparison of label-free, metabolic labeling, and isobaric chemical labeling for quantitative proteomics on LTQ Orbitrap Velos. *J Proteom Res* **11:** 1582–1590.

Li, Z., Wang, Y., Yao, Q., Justice, N.B., Ahn, T.H., Xu, D., *et al*. (2014) Diverse and divergent protein post-translational modifications in two growth stages of a natural microbial community. *Nat Commun* **5:** 4405.

Lu, W., Bennett, B.D., and Rabinowitz, J.D. (2008) Analytical strategies for LC–MS-based targeted metabolomics. *J Chromatogr B* **871:** 236–242.

Lu, W., Clasquin, M.F., Melamud, E., Amador-Noguez, D., Caudy, A.A., and Rabinowitz, J.D. (2010) Metabolomic analysis via reversed-phase ion-pairing liquid chromatography coupled to a stand alone orbitrap mass spectrometer. *Anal Chem* **82:** 3212–3221.

Luo, B., Groenke, K., Takors, R., Wandrey, C., and Oldiges, M. (2007) Simultaneous determination of multiple intracellular metabolites in glycolysis, pentose phosphate pathway and tricarboxylic acid cycle by liquid chromatography–mass spectrometry. *J Chromatogr A* **1147:** 153–164.

Martens, L., Chambers, M., Sturm, M., Kessner, D., Levander, F., Shofstahl, J., *et al*. (2011) mzML – a community standard for mass spectrometry data. *Mol Cell Proteom* **10:** R110.000133.

McCutcheon, J.P., and Moran, N.A. (2012) Extreme genome reduction in symbiotic bacteria. *Nat Rev Microbiol* **10:** 13–26.

Melamud, E., Vastag, L., and Rabinowitz, J.D. (2010) Metabolomic analysis and visualization engine for LC−MS data. *Anal Chem* **82:** 9818–9826.

Miflin, B.J., and Habash, D.Z. (2002) The role of glutamine synthetase and glutamate dehydrogenase in nitrogen assimilation and possibilities for improvement in the nitrogen utilization of crops. *J Exp Bot* **53:** 979–987.

Morris, S.M., Jr. (2002) Regulation of enzymes of the urea cycle and arginine metabolism. *Annu Rev Nutr* **22:** 87–105.

Naito, M., Morton, J.B., and Pawlowska, T.E. (2015) Minimal genomes of mycoplasma-related endobacteria are plastic and contain host-derived genes for sustained life within Glomeromycota. *Proc Natl Acad Sci USA* **112:** 7791–7796.

Nesvizhskii, A.I., and Aebersold, R. (2005) Interpretation of shotgun proteomic data the protein inference problem. *Mol Cell Proteom* **4:** 1419–1440.

Ohshima, S., Sato, Y., Fujimura, R., Takashima, Y., Hamada, M., Nishizawa, K., *et al*. (2016) Mycoavidus cysteinexigens gen. nov., sp. nov., an endohyphal bacterium isolated from a soil isolate of the fungus *Mortierella elongata*. *Int J Syst Evol Microbiol* **66:** 2052–2057.

Pan, C., Fischer, C.R., Hyatt, D., Bowen, B.P., Hettich, R.L., and Banfield, J.F. (2011) Quantitative tracking of isotope flows in proteomes of microbial communities. *Mol Cell Proteomics* **10:** 006049–00M110.

Pan, C., Kora, G., McDonald, W.H., Tabb, D.L., VerBerkmoes, N.C., Hurst, G.B., *et al*. (2006) ProRata: a quantitative proteomics program for accurate protein abundance ratio estimation with confidence interval evaluation. *Anal Chem* **78:** 7121–7131.

Rabinowitz, J.D., and Kimball, E. (2007) Acidic acetonitrile for cellular metabolome extraction from *Escherichia coli*. *Anal Chem* **79:** 6167–6173.

Salvioli, A., Chiapello, M., Fontaine, J., Hadj-Sahraoui, A.L., Grandmougin-Ferjani, A., Lanfranco, L., and Bonfante, P. (2010) Endobacteria affect the metabolic profile of their host Gigaspora margarita, an arbuscular mycorrhizal fungus. *Environ Microbiol* **12:** 2083–2095.

Salvioli, A., Ghignone, S. Novero, M., Navazio, L., Venice, F., Bagnaresi, P., and Bonfante, P. (2016) Symbiosis with an endobacterium increases the fitness of a mycorrhizal fungus, raising its bioenergetic potential. *ISME J* **10:** 130–144.

Shakya, M., Gottel, N., Castro, H., Yang, Z.K., Gunter, L., Labbe, J., *et al*. (2013) A multifactor analysis of fungal and bacterial community structure in the root microbiome of mature *Populus deltoides* trees. *PLoS One* **8:** e76382.

Sharma, M., Schmid, M., Rothballer, M., Hause, G., Zuccaro, A., Imani, J., *et al*. (2008) Detection and identification of bacteria intimately associated with fungi of the order Sebacinales. *Cell Microbiol* **10:** 2235–2246.

Steffen, M.M., Dearth, S.P., Dill, B.D., Li, Z., Larsen, K.M., Campagna, S.R., and Wilhelm, S.W. (2014) Nutrients drive transcriptional changes that maintain metabolic homeostasis but alter genome architecture in microcystis. *ISME J* **8:** 2080–2092.

Torres-Cortes, G., Ghignone, S., Bonfante, P., and Schussler, A. (2015) Mosaic genome of endobacteria in arbuscular mycorrhizal fungi: transkingdom gene transfer in an ancient mycoplasma-fungus association. *Proc Natl Acad Sci USA* **112:** 7785–7790.

Vannini, C., Carpentieri, Salvioli, A., Novero, A., Marsoni, M., Testa, M.L., de Pinto, M., *et al.* (2016) An interdomain network: the endobacterium of a mycorrhizal fungus promotes antioxidative responses in both fungal and plant hosts. *New Phytol* **211:** 265–275.

Wang, Y., Ahn, T.H., Li, Z., and Pan, C. (2013) Sipros/ProRata: a versatile informatics system for quantitative community proteomics. *Bioinformatics* **29:** 2064–2065.

Wang, Y., Kora, G., Bowen, B.P., and Pan, C. (2014) MIDAS: a database-searching algorithm for metabolite identification in metabolomics. *Anal Chem* **86:** 9496–9503.
Washburn, M.P., Wolters, D., and Yates, J.R. (2001) Large-scale analysis of the yeast proteome by multidimensional protein identification technology. *Nat Biotechnol* **19:** 242–247.
Waterman-Storer, C.M. (2001). Microtubule/organelle motility assays. *Curr Protoc Cell Biol* Chapter 13: Unit 13 11.
Wiśniewski, J.R., Zougman, A., Nagaraj, N., and Mann, M. (2009) Universal sample preparation method for proteome analysis. *Nat Methods* **6:** 359–362.
Wu, C.C., and MacCoss, M.J. (2002) Shotgun proteomics: tools for the analysis of complex biological systems. *Curr Opin Mol Ther* **4:** 242–250.
Yao, Q., Bollinger, C., Gao, J., Xu, D., and Thelen, J.J. (2012) P(3)DB: an integrated database for plant protein phosphorylation. *Front Plant Sci* **3:** 206.
Yao, Q., Ge, H., Wu, S., Zhang, N., Chen, W., Xu, C., et al. (2014) P(3)DB 3.0: from plant phosphorylation sites to protein networks. *Nucleic Acids Res* **42 (Database issue):** D1206–D1213.
Zhao, Y., Park, R.D., and Muzzarelli, R.A. (2010) Chitin deacetylases: properties and applications. *Mar Drugs* **8:** 24–46.
Zientz, E., Dandekar, T., and Gross, R. (2004) Metabolic interdependence of obligate intracellular bacteria and their insect hosts. *Microbiol Mol Biol Rev* **68:** 745–770.

Supporting information

Additional Supporting Information may be found in the online version of this article at the publisher's web-site:

Table S1. Summary statistics of up-regulated and down-regulated protein abundances, PTM fractional occupancies and metabolite concentrations between two conditions, with p values < 0.05 and q values < 0.05. The comparisons were between nitrogen-poor growth condition with a suppressed endobacterial population (N−B−), nitrogen-poor growth condition with a normal endobacterial population (N−B+), nitrogen-rich growth condition with a suppressed endobacterial population (N+B−) and nitrogen-rich growth condition with a normal endobacterial population (N+B+).
Table S2. Biosynthesis and import of amino acids by the active endobacterium. TCA: citric acid cycle. PPP: pentose phosphate pathway.
Fig. S1. Growth curves of the *M. elongata* AG-77 in the following four conditions: nitrogen-poor growth condition with a suppressed endobacterial population (N−B−), nitrogen-poor growth condition with a normal endobacterial population (N−B+), nitrogen-rich growth condition with a suppressed endobacterial population (N+B−) and nitrogen-rich growth condition with a normal endobacterial population (N+B+). Error bars represent one standard deviation of biomasses.
Fig. S2. Base peak ion chromatograms and composite mass spectra of all metabolomics runs.
Fig. S3. A. Purine biosynthetic pathway of the endobacterium *Mycoavidus* sp. Arrows indicate enzymatic reactions and direction of reaction. B. Pyrimidine biosynthetic pathway of the endobacterium *Mycoavidus* sp. Arrows indicate enzymatic reactions and direction of reaction.
Fig. S4. Pentose phosphate pathway. Arrows indicate enzymatic reactions and direction of reaction.
Fig. S5. Conservation of a phosphorylation event on pyruvate dehydrogenases from different organisms. Partial sequences of the pyruvate dehydrogenases are shown. The number preceding each sequence represents the position of the first amino acid of the sequence on its associated protein. Phosphorylated serine residue in each organism is highlighted in red.
Fig. S6. Intracellular lipids (IL) produced in *M. elongata* AG-77 hyphae (H) in the four conditions. Lipids were stained by Nile Red and then visualized by confocal microscopy.
Supplementary Data 1: Proteins identified in each growth condition.
Supplementary Data 2: PTMs identified in each growth condition.
Supplementary Data 3: Metabolites identified in each growth condition.
Supplementary Data 4. Proteins with statistically significant abundance changes between two different conditions.
Supplementary Data 5. PTMs' fraction occupancies with statistically significant changes between two different conditions.
Supplementary Data 6. Metabolites with statistically significant abundance changes between two different conditions.